Composites: Part B 44 (2013) 501–507

Contents lists available at SciVerse ScienceDirect

Composites: Part B

journal homepage: www.elsevier.com/locate/compositesb

Predicting nonlinear stress–strain curves of unidirectional fibrous composites in consideration of stick–slip

M.M.S. Dwaikat [a,*], C. Spitas [a], V. Spitas [b]

[a] Faculty of Industrial Design Engineering, Technical University of Delft, Delft, The Netherlands
[b] Machine Elements Laboratory, Faculty of Mechanical Engineering, National Technical University of Athens, Athens, Greece

ARTICLE INFO

Article history:
Received 17 November 2011
Received in revised form 23 January 2012
Accepted 23 March 2012
Available online 5 April 2012

Keywords:
A. Fibers
B. Fiber/matrix bond
B. Mechanical properties
C. Micromechanics
B. Plastic deformation

ABSTRACT

A simple and efficient methodology is developed for computing nonlinear stress–strain curve of unidirectional fibrous nano-composites loaded in the direction of the perfectly aligned fibers. The method, based on shear lag analysis and derived from basic principles of continuum micromechanics, incorporates shear stick–slip constitutive law at the fiber–matrix interface. The matrix is modeled as elastic–plastic with linear isotropic strain hardening. The approach thus predicts the nonlinear behavior of the composite stress–strain curve due to both interfacial shear slippage of reinforcement fibers within the matrix and due to spread of plasticity within the matrix. The proposed method is compared to experimental results on aligned fibrous nano-composites and very good agreement is obtained when low values of interfacial shear strength are used. The study shows that when the interfacial bond between the matrix and the fiber is strong, higher stress concentration leads to spread of plasticity in the composite at lower bulk strains. However, when the bond is weak, interfacial slippage causes a relief in the accumulation of stress in the matrix. Both factors seem to provide reasonable explanation for the observed nonlinearity and improved stiffness of the composite. A set of parametric studies is also performed and the proposed method is compared to existing models.

1. Introduction

The discovery of Carbon Nanotubes (CNTs) in early 1990s opened many doors for their potential use in nano-composite materials and that is due to their superior and unique characteristics. Many attempts were made for predicting the elastic modulus of nano-composites, and those ranged from simplified hand-calculation methods to complex and detailed numerical finite element/difference methods. A comprehensive survey of the methods used for modeling nano-composites can be found in Hu et al. [1]. Most of these methods provide only the initial tangent stiffness of the composite and do not fully capture the nonlinear behavior of the composite due to slippage of the nano-fiber reinforcements or due to the yielding of the constituents. This is mainly because either full bond or partial bond was assumed between the fibers and matrix. The methods that assume a realistic interaction between fibers and matrix (such as frictional–stick–slip) resulted in complex finite difference equations for the response that are difficult and time-consuming to solve.

Atomic Force Microscopic (AFM) techniques revealed that because of the nature of graphite surface (of which the CNT are made) an AFM tip, when pressed on the graphite surface, moves in a stick–slip manner with sliding occurring suddenly when the applied load exceeds certain threshold [2,3]. This can be attributed to the geometrical configuration of the carbon atoms of the graphite surface with the regular grid of high-low potentials. Given this behavior one can speculate that a stick–slip motion is also possible on the points of contact between the polymer chains and the graphite surface of the CNTs. Spitas and Spitas [4] explained a stick–slip behavior of nano-composite and showed that the interface stick–slip behavior affects the nonlinearity, and thus the hysteresis, of the nano-composite. From the finite element simulations [4] of a representative volume element 'RVE', it was found that the shear slip is maximal at the fiber tip and reduces drastically as we go towards the center of the fiber. This interfacial slippage provides a mechanism through which the energy can be dissipated and thus leads to a better damping behavior of the nano-composite [5]. The shear stress at the interface will increase with the slippage until the adhesion/bond strength between the CNT and the matrix is exceeded then sliding is initiated thus releasing the interface energy [6–8].

A comprehensive survey of the methods used for modeling nano-composites can be found in [3,14]. Most existing models assume either full or partial bond between the fibers and matrix. Among the famous methods used to model nano-composites are

* Corresponding author. Tel.: +31 6 8334 8290.
E-mail address: m.m.s.dwaikat@tudelft.nl (M.M.S. Dwaikat).

1359-8368/$ - see front matter © 2012 Elsevier Ltd. All rights reserved.
http://dx.doi.org/10.1016/j.compositesb.2012.03.019

the Mori–Tanaka model that is based on Eshelby inclusion theory and Halpin-Tsai model that is an interpretation of Hill's potential theory. A thorough review of these models can be found in [3,9–15]. These models seem to be universal in their assumptions and can account for various configurations of fiber aspect ratio, fiber orientation, volume fraction, and elastic properties of the different phases in the composite. However, they only generate initial tangent elastic moduli of the composite (Young and Shear moduli in orthotropic scenario) and do not trace the nonlinearity in the stress–strain curve of the composite. Further, in these models, the interaction between the fibers and the matrix is generally accounted for through empirically-determined efficiency factors. In addition, incorporating the nonlinear effects of plasticity or stick–slip at the interface in these models is cumbersome and requires fundamental revision. The methods that assume a realistic interaction between fibers and matrix (such as frictional–stick–slip, shear lag models, and interphase models) generally lead to complex finite difference equations for the response that are difficult and time-consuming to solve. Such complexity of existing models makes them even more tedious for use on the macro-scale modeling through the computationally demanding stochastic finite element methods, for instance.

Motivated by the need to have an efficient and computationally fast approach for modeling the nonlinear behavior of fibrous nano-composites, the authors sought to develop a simplified analytical model for predicting nonlinear stress–strain curve of unidirectional fibrous nano-composites. The proposed model is derived from basic principles of equilibrium and compatibility of unidirectional fibers and takes into account the effect of length and diameter of the fiber, volume fraction and mechanical properties of the constituents. Thus, the model can accommodate different types of carbon nanotubes (either single-walled 'SWCNT' or multi-walled 'MWCNT') by adopting their relevant elastic properties. The simplicity of the proposed model, compared to other complex models, makes it attractive for incorporation in multi-scale stochastic finite element analysis, which demands extensive numerical computations. Thus, the proposed model is one step towards a holistic approach for modeling and design of nano-composites.

2. Proposed model

Consider, as shown in Fig. 1a, a representative volume element (RVE) in the shape of a composite cylinder of outer radius R that has an embedded fiber of radius r_f and length L. When the RVE is loaded uniformly in the direction of the fiber, strain and stress incompatibilities arise between the fiber and matrix due to the difference in elastic properties. In case of nano-composites containing carbon nanotubes, these incompatibilities are significant due to the high order of magnitude difference in the elastic moduli of the composites phases. The concept of stick–slip behavior can be summarized as follows. Longitudinal stress $\sigma_x^f(x)$ is transferred to the fiber through the interfacial shear $\tau_i(x)$ which varies along the length of the fiber. This interfacial shear stress causes gradual relative deformation, $u_s(x)$, at the interface between the fiber and the matrix. Once the interfacial shear stress exceeds a critical value τ_c, termed as the interfacial shear strength 'IFSS', relative sliding occurs at the interface where u_s increases under constant shear stress τ_c, This phenomenon, alongside with the plasticity in the matrix that occurs due to stress concentration, will be used to model the nonlinearity in the composite stress–strain behavior.

Isolating the components of the RVE, equilibrium equations can be written for both the fiber and the matrix. These equations are then related through material constitutive relationships. Compatibility condition similar to that adopted by Cox [14] is used to derive governing equations of the interfacial shear slippage, which upon solving, give rise to the stress and strain distribution within the RVE. Homogenization technique is then used to derive the stress–strain behavior of the composite.

3. Governing equations

For the purpose of simplicity, and as shown in Fig. 2, the stress field in the matrix and fiber will be takento be uniform over the radial and circumferential directions, and thus we have an axisymmetric case where the stresses are dependent only on the longitudinal distance x.

3.1. Equilibrium of phases

Referring to Fig. 1b the equilibrium equations in the longitudinal direction for the fiber can be written as:

$$\left(\sigma_f + \frac{\partial \sigma_f}{\partial x} dx\right)\pi r_f^2 + 2\pi r_f \tau_i(u_s)dx - \sigma_f \pi r_f^2 = 0 \tag{1}$$

$$\frac{\partial \sigma_f}{\partial x} = -\frac{2}{r_f}\tau_i(u_s) \tag{2}$$

Similarly for the matrix we have

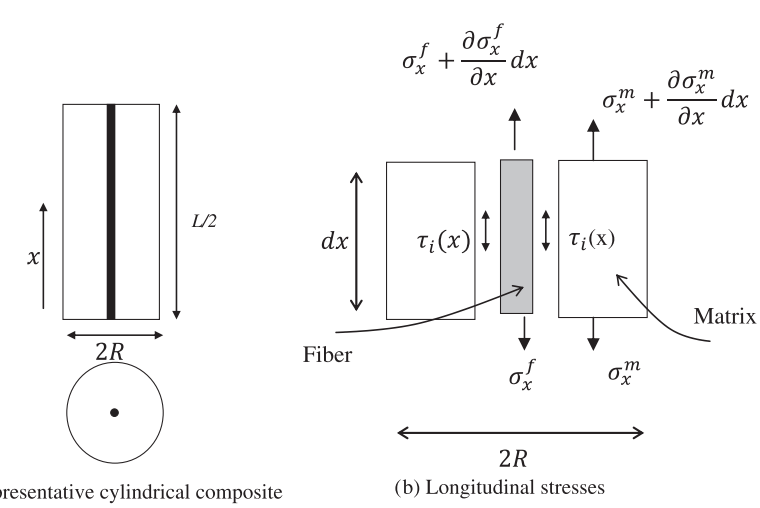

Fig. 1. The longitudinal stresses in a representative composite cylinder.

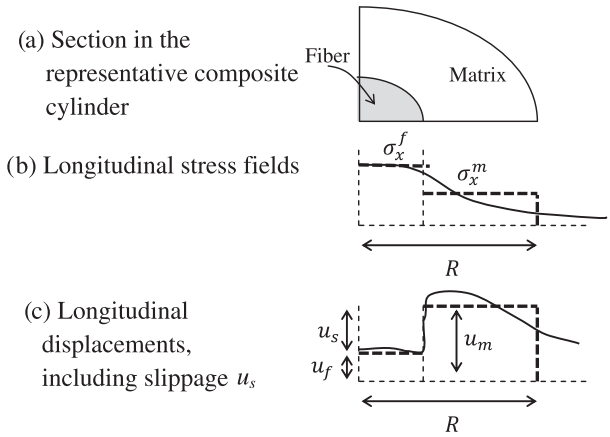

Fig. 2. Longitudinal stress and displacement fields.

$$\left(\sigma_m + \frac{\partial \sigma_m}{\partial x} dx\right)\pi\left(R^2 - r_f^2\right) - 2\pi r_f \tau_i(u_s)dx - \sigma_m \pi\left(R^2 - r_f^2\right) = 0 \tag{3}$$

$$\frac{\partial \sigma_m}{\partial x} = \frac{2r_f}{\left(R^2 - r_f^2\right)}\tau_i(u_s) \tag{4}$$

3.2. Kinematic relationships

The compatibility condition that needs to be satisfied along the fiber is that the displacement in the matrix should equal the displacement in the fiber plus the slippage that occurs at the interface (Fig. 2c). i.e.;

$$u_m(x) = u_f(x) + u_s(x) \tag{5}$$

which upon differentiation with respect to x gives the relation between the strains as:

$$\varepsilon_m(x) = \varepsilon_f(x) + \frac{du_s}{dx} \tag{6}$$

3.3. Constitutive relationships

The matrix is assumed to follow a bi-linear elastic–plastic behavior with isotropic strain hardening rule as shown in Fig. 3a. Neglecting Poisson's ratio, the elastic–plastic constitutive law can be written as:

$$\sigma_m = \begin{cases} E_m \varepsilon_m, & \varepsilon_m < \varepsilon_Y \\ E_{sh}\varepsilon_m + (E_m - E_{sh})\varepsilon_Y, & \varepsilon_m > \varepsilon_Y \end{cases} \tag{7}$$

E_m is the Young modulus of the matrix, E_{sh} is the slope of the strain hardening segment of the stress–strain curve, and ε_Y is the strain at yield. Differentiating σ_m with respect to x and substituting the kinematic relationship (Eq. (6)) between fiber and matrix strain:

$$\frac{d\sigma_m}{dx} = \begin{cases} E_m\left(\frac{\partial^2 u_f}{\partial x^2} + \frac{\partial^2 u_s}{\partial x^2}\right), & \varepsilon_m < \varepsilon_Y \\ E_{sh}\left(\frac{\partial^2 u_f}{\partial x^2} + \frac{\partial^2 u_s}{\partial x^2}\right) + (E_m - E_{sh})\frac{d\varepsilon_Y}{dx}, & \varepsilon_m > \varepsilon_Y \end{cases} \tag{8}$$

The fiber is assumed to remain elastic, which is justified for carbon nanotubes that have very high yield strength compared to the matrix. Thus:

$$\sigma_f = E_f \varepsilon_f \tag{9}$$

which upon differentiation with respect to x and substituting the kinematic relationship above gives:

$$\frac{\partial \sigma_f}{\partial x} = E_f \frac{\partial^2 u_f}{\partial x^2} \tag{10}$$

The stick–slip behavior is quite complex, therefore an idealized constitutive law that describes the relation between interfacial shear τ_i and relative interfacial slippage u_s will be used. As shown in Fig. 3b, an idealized stick–slip law is considered to be bi-linear, where "slippage" occurs after a threshold shear stress is reached [4]:

$$\tau_i(u_s) = \begin{cases} \frac{\tau_c}{u_c}u_s, & \frac{u_s}{u_c} < 1 \\ \tau_c, & \frac{u_s}{u_c} \geqslant 1 \end{cases} \tag{11}$$

The value of u_c represents the critical relative deformation after which slippage takes place at the interface with constant shear resistance τ_c. If we consider the elastic modulus of the matrix E_m to be isotropic, then the value of u_c can be taken as the deformation that occurs once the shear stress at the interface causes yielding of the matrix shell at the interface, and thus u_c can be computed as:

$$u_c = \alpha(R - r_f)F_{sm}\frac{2(1+\mu)}{E_m} \tag{12}$$

where F_{sm} is the shear strength of the matrix, and $\alpha(R - r_f)$ represents the thickness of the matrix shell layer where the shear slippage is assumed to take place. μ is the Poisson's ratio of the matrix material.

3.4. General equation and numerical solution

By substituting the derivatives of the constitutive laws into the equilibrium equations, two differential equations with two unknowns (namely, u_s and u_f) will emerge. Eliminating u_f leads to the following second order differential equation:

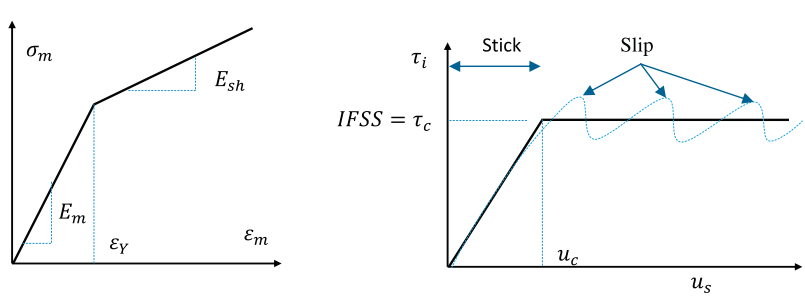

(a) Bi-linear plasticity model

(b) Idealized stick-slip constitutive law

Fig. 3. Constitutive relationships for the matrix and the interface.

$$\frac{\partial^2 u_s}{\partial x^2} + \frac{2\pi r_f \tau_i(u_s)}{E_* \pi (R^2 - r_f^2)} - \frac{2\pi r_f \tau_i(u_s)}{E_f \pi r_f^2} + \left(\frac{E_m - E_*}{E_*}\right)\frac{\partial \varepsilon_Y}{\partial x} = 0 \tag{13}$$

where $E_* = E_m$ in case $\varepsilon_m < \varepsilon_Y$ and $E_* = E_{sh}$ in case $\varepsilon_m > \varepsilon_Y$.

The equation above is nonlinear and in order to solve it, an iterated finite difference scheme is employed. Discretizing space using: $x_k = k\Delta x$, $k = 1, 2, \ldots, N$ where $\Delta x = L/N$, the solution for the slippage at location $k + 1$ can be obtained using:

$$u_s^{k+1} = \left\{\frac{2\pi r_f \tau_i(u_s^k)}{E_f \pi r_f^2} - \frac{2\pi r_f \tau_i(u_s^k)}{E_* \pi (R^2 - r_f^2)} - \left(\frac{E_m - E_*}{E_*}\right)\frac{d\varepsilon_Y}{dx}\right\}(\Delta x)^2 + 2u_s^k - u_s^{k-1} \tag{14}$$

For propagating the solution u_s^{k+1} using the finite difference scheme above, two boundary conditions are needed and these relate to $u_s^0 = u_s|_{x=0}$ and $u_s^1 = u_s^0 + \Delta x \frac{du_s}{dx}|_{x=0}$. The value of $d\varepsilon_Y/dx$ represents the change in the yield surface of the matrix material, and thus is calculated from the previous load step as $(\varepsilon_Y^k - \varepsilon_Y^{k-1})/\Delta x$.

The strain in the fiber is obtained by backward finite difference scheme for the combination of Eqs. (2) and (10):

$$u_f^{N-k-1} = -\frac{2(\Delta x)^2}{E_f r_f}\tau_i(u_s^{N-k}) + 2u_f^{N-k} - u_f^{N-k+1} \tag{15}$$

With the boundary condition imposed at the far end of the fiber $u_f^N = u_f|_{x=L}$ and $u_f^{N-1} = u_f^N - \Delta x \frac{du_f}{dx}|_{x=L}$. It must be noted that the model proposed above focuses on presenting the solution in terms of the interfacial slippage, rather than in terms of the force or stress in the fiber as commonly followed in most shear-lag models reported in literature. Therefore, the boundary conditions written above, consist of two sets: The first set pertains to the slip differential equation (Eq. (14)), while the second set pertains to the solution of displacement field in the fiber (Eq. (15)). Each set requires two boundary conditions since the equations are of the second order.

The first set of boundary conditions has an influence on the state of interfacial slip distribution, i.e., whether the slip has initiated at the boundary or not. For each assumed value of initial boundary slip, a distribution of slip is obtained via Eq. (14), and this slip distribution gives rise to the rest of the terms (strains and stresses in the composite phases) which in turn gives a point (strain, stress) on the composite stress–strain curve. Thus, this set of boundary conditions has no influence on the shape of the stress–strain curve of the composite, however, it affects the starting point of the composite stress–strain curve in the solution. When the values used in this set of boundary conditions are small, the resulting interfacial slip is minor and thus the composite response is in the elastic range. However, if the values are large, significant slippage is propagated and thus high stresses occur in the composite phases in order to equilibrate such high interfacial shear. Therefore, it is recommended to start with very small values of boundary conditions. Of course, since the equations are solved via finite difference scheme, the value of this set boundary conditions depends on the critical shear slippage value u_c (in Eq. (12)). Generally, a starting step of the order $10^{-3} \times u_c$ is recommended for u_s^0 based on numerical analysis conducted by the authors.

The second set of boundary conditions affects the nature of interaction at the fiber–matrix interface. In the current study, the authors used the conventional boundary condition similar to that adopted by Cox [15] in the first micromechanics shear-lag model, i.e. zero stress at the far end, which corresponds to the model proposed above as: $\frac{du_f}{dx}|_{x=L} = 0$ and $u_f|_{x=L} = u_s|_{x=L}$. This type of boundary conditions was confirmed by experimental evidence on short Kevlar fibers embedded in epoxy resins [16]. Therefore, this boundary conditions is commonly used in micromechanics modeling of fibrous composites.

Once the solutions u_s^k and u_f^k are known, the strains and the corresponding stresses in the matrix and the fiber can be readily computed by backward substitution. The overall equilibrium equation is repeatedly checked until the residual error is below a tolerance value δ:

$$\pi r_f^2 \frac{\partial \sigma_f}{\partial x} + \pi(R^2 - r_f^2)\frac{\partial \sigma_m}{\partial x} \leqslant \delta \tag{16}$$

$$\sigma_f^k - \sigma_f^{k-1} + \frac{\pi(R^2 - r_f^2)}{\pi r_f^2}\left(\sigma_m^k - \sigma_m^{k-1}\right) \leqslant \frac{\Delta x}{\pi r_f^2}\delta \tag{17}$$

3.5. Homogenization and composite stress–strain curve

The properties of the nano-composite are homogenized by averaging the stresses and strains over the RVE. Thus the average strains and stresses in the fiber and in the matrix are computed as:

$$\sigma_{f,m}^{Av} = \frac{1}{L}\int_0^L \sigma_{f,m}(x)dx \text{ and } \varepsilon_{f,m}^{Av} = \frac{1}{L}\int_0^L \varepsilon_{f,m}(x)dx \tag{18}$$

The average total stress and strain is obtained as a result of contribution for the difference constituents, i.e.;

$$L(A_m + A_f)\sigma_{total}^{Av} = \int_0^L (A_m\sigma_m(x) + A_f\sigma_f(x))dx$$
$$\text{and } L(A_m + A_f)\varepsilon_{total}^{Av} = \int_0^L (A_m\varepsilon_m(x) + A_f\varepsilon_f(x))dx \tag{19}$$

Which leads to:

$$\sigma_{total}^{Av} = \varphi\sigma_f^{Av} + (1-\varphi)\sigma_m^{Av} \text{ and } \varepsilon_{total}^{Av} = \varphi\varepsilon_f^{Av} + (1-\varphi)\varepsilon_m^{Av} \tag{20}$$

where $\varphi = A_f/(A_m + A_f) = r_f^2/R^2$ is assumed to represent the fiber volume fraction.

4. Comparison to experimental data

The proposed approach is compared against published test data [17] on aligned fibrous nano-composites. Fig. 4 compares predictions from the proposed model against stress–strain curves obtained experimentally for PEEK–MWCNT nano-composites with different MWCNT volume fractions (6% and 10%). The MWCNT were injected into PEEK melts and then molded in thin films. Results of focused ion beam scanning "FIB" showed very good alignment of MWCNT in the direction of injection [17]. The average diameter of the nanotubes was 40 nm and the average aspect ratio was 150. The average measured elastic modulus and yield strength of the PEEK was reported as 4.2 GPa and 68 MPa, respectively, while the elastic modulus of the MWNT was assumed as 1 TPa by adopting it from Ref. [17]. The IFSS (i.e., τ_c) of the MWCNT were estimated from a simplified shear lag analysis by Ogasawara et al. [17] and was found to be between 2 and 6 MPa. Further, recent experimental work [18] using direct pull-out tests has shown that the interfacial shear strength between MWCNT and PEEK ranges between 3.5 and 7 MPa. Using interfacial shear strength of 6 MPa produces better agreement with the test data as shown in Fig. 4, which compares the predicted stress–strain curves of the PEEK–CNT against the test data for different fiber volume fraction. The higher the value of IFSS, the greater the initial tangent stiffness of the composite. However, higher values of IFSS leads to higher stresses in the matrix and thus earlier plasticity, especially near the far ends of the fiber. Nonlinearity in the nano-composite behavior emerges due the combination of interfacial slippage and spread of plasticity in the matrix.

For further verification of the validity of the proposed approach, another comparison is conducted against published test data [19]

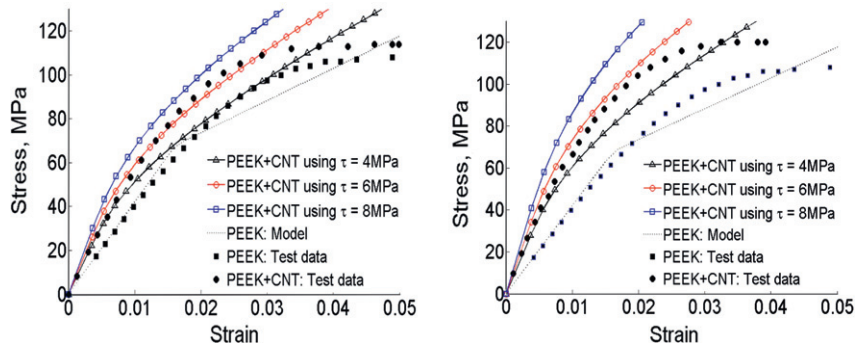

(a) PEEK-CNT (with 6% vol. fraction) (b) PEEK-CNT (with 10% vol. fraction)

Fig. 4. Predictions from the proposed model compared to test data on PEEK–MWCNT nano-composite.

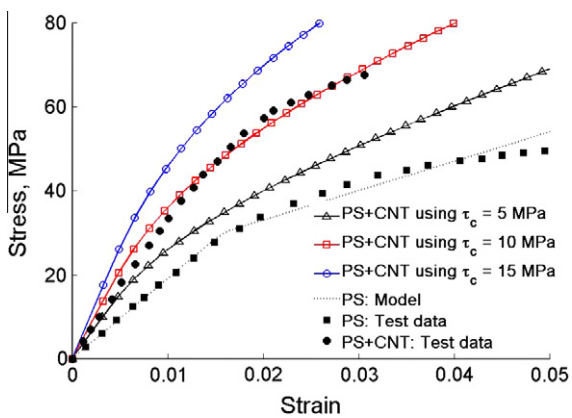

Fig. 5. Predictions from the model against test data on PS–MWCNT nano-composite (5 wt%.) – using high aspect ratio of 200.

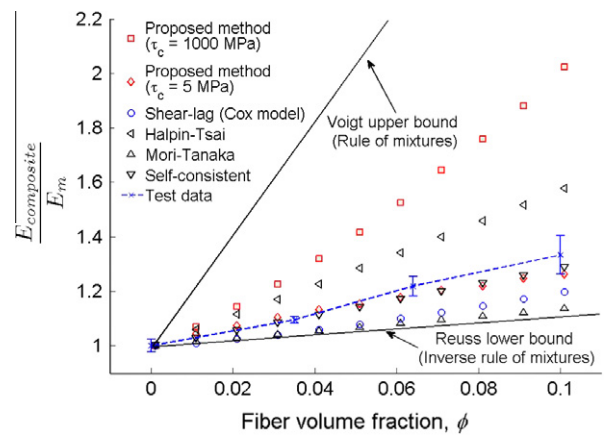

Fig. 6. Predictions from different methods compared to test data on PEEK–CNF nano-composite.

on MWCNT-reinforced Polystyrene (PS) nano-composite and this is shown in Fig. 5. In the experiment reported in [19], MWCNT were injected into molten PS matrix and the nano-composite is molded into thin sheets, which were immediately subjected to uniaxial stretching, thus causing greater degree of alignment of the CNT within the PS. Dispersion of the nanotubes was ensured by sonication of the PS–CNT melt. Predictions from the proposed approach are plotted in Fig. 5 against results from the experiment. Different values of IFSS were used and it seems higher degree of interaction (IFSS $\sim$ 10 MPa) exists between PS and CNT in that experiment, as compared to PEEK–CNT nano-composite (IFSS $\sim$ 5 MPa). The differences can very well be attributed to differences in the CNT type and quality, manufacturing process, degree of alignment, and to the differences in the chemical interaction between the polymers and the CNT chains.

Yet, another comparison between predictions from the proposed model and experimental results [20] on initial tangent stiffness of PEEK–CNF nano-composite is shown in Fig. 6. The comparison also includes the predictions from different methods including shear lag (Cox model), Halpin-Tsai, Mori–Tanaka, and self-consistent methods in addition to Voigt and Reuss upper and lower bounds. In the experiments reported by Ref. [20], different volume fractions of CNF with small aspect ratio ($\sim$10) were injected into molten PEEK and then nano-composite films were prepared by the means of co-rotating twin-screw extruder. Good degree of alignment due to the extrusion process is reported. The Young modulus of the CNF is much lower than CNT and direct measurement [21] showed that it ranges from 5 to 90 GPa. In the reported study, the authors stated that for CNF with similar characteristics like those adopted in their study, the value of E_f is estimated to range between 19 and 280 GPa. Based on these reports, an average value of 90 GPa is selected for E_f and the analysis is conducted using two different values of IFSS as shown in Fig. 6, namely a value of τ_c = 1000 MPa representing very good interaction between CNF and PEEK and a value of τ_c = 5 MPa representing a deteriorated interaction. Better agreement with test data is obtained when a value of IFSS $\sim$ 5 MPa is used which indicates a typical interaction between the matrix and the fibers as it was the case with the previous MWCNT and PEEK nano-composites.

Fig. 6 also compares results from the proposed method and results from different methods for evaluating the composite tangent elastic modulus. The figure shows that the proposed method compares very well with other methods, particularly with the self-consistent method. An advantage of the proposed method in addition to its simplicity is that it takes explicit consideration of the interfacial shear strength, and thus the interaction at the fiber–matrix interface on the composite elastic modulus. Further, the proposed method is capable of generating the nonlinear stress–strain curve of the composite considering the propagation of interfacial slippage and the spread of plasticity. Such feature is challenging to implement in the more complex models, such as the Mori–Tanaka or self-consistent methods. These methods only generate the initial tangent elastic modulus of the composite and require amending in case the nonlinear (plastic or viscoelastic) tangent modulus is required.

The influence of fiber aspect ratio on the composite elastic modulus is shown in Fig. 7. All models converge to the rule of mixtures for higher aspect ratios. As expected, the proposed model converges very fast to the rule of mixture solution when the IFSS is high. In Fig. 8 we study the influence of the constituent stiffness

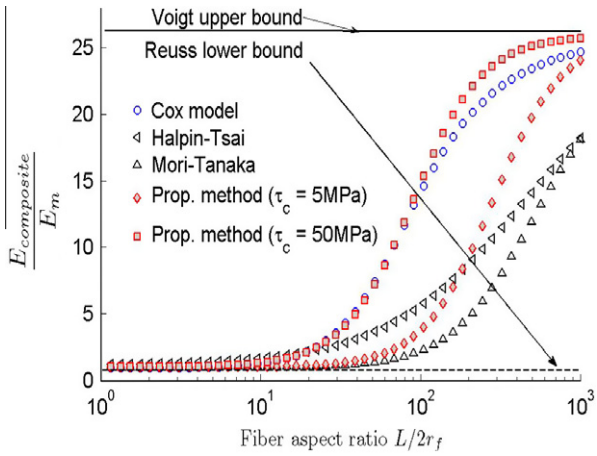

Fig. 7. Effect of fiber aspect ratio (τ_c = 10 MPa, φ = 0.1, E_f/E_m = 250).

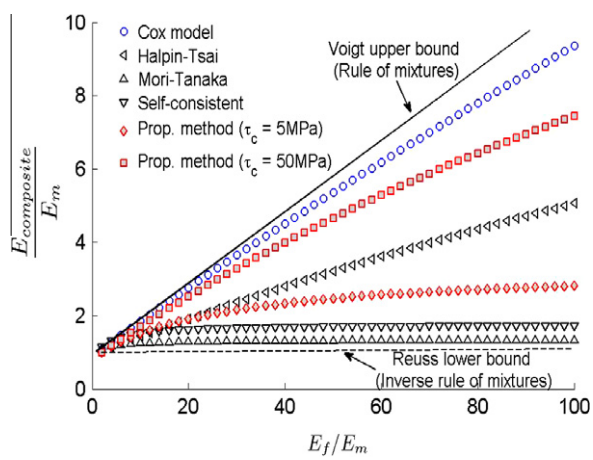

Fig. 8. Effect of stiffness ratio on the composite elastic modulus (L/d = 200; phi = 10%).

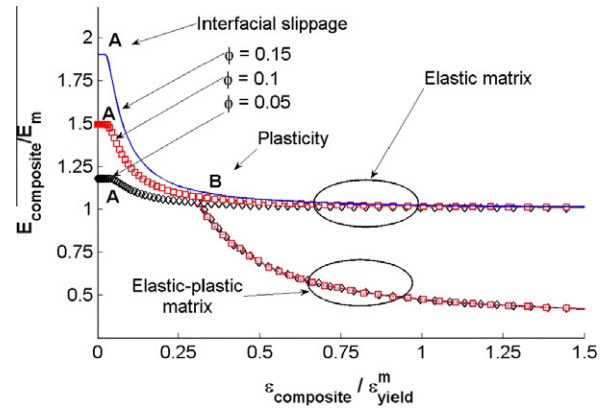

Fig. 9. Predicted composite tangent stiffness using different values of fiber volume fraction.

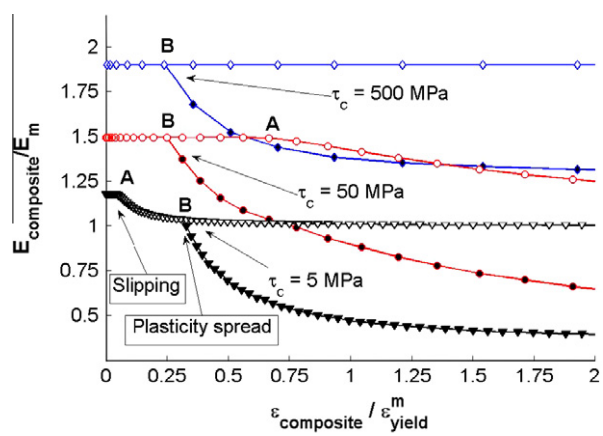

Fig. 10. Predicted composite tangent stiffness using different values of IFSS (● ♦ ▼: assuming elastic–plastic matrix, ○ ◇ ▽ assuming elastic matrix).

ratios on the predicted composite elastic modulus. When the E_f/E_m ratio is small, the predictions converge to Voigt upper bound limit. This is expected because when the constituent materials have comparable stiffness, the stress and strain distributions in the composite will tend to be more uniform, which is what the rule of mixtures solution is based on.

The nonlinearity in the composite behavior is studied in Figs. 9 and 10 by tracing the tangent stiffness of the composite $\left\{\frac{d\sigma^{Av}_{total}}{d\varepsilon^{Av}_{total}}\right\}$ as a function of the composite strain $\{\varepsilon^{Av}_{total}\}$. In the analysis, two scenarios were considered, the first is using fully elastic matrix, and the second is using elasto-plastic matrix. When the matrix is assumed to be fully elastic, the only source for nonlinearity (i.e., the reduction in $\frac{d\sigma^{Av}_{total}}{d\varepsilon^{Av}_{total}}$) is the interfacial shear slippage, which is seen to occur at low strains (at point A in Figs. 9 and 10). When the matrix is considered as elasto-plastic, further and dramatic reduction in composite tangent stiffness is initiated (as can be seen at point B in Figs. 9 and 10). This further reduction is the result of the localized concentration of stresses in the matrix at the far ends of the RVE where interfacial shear stress is highest. Increasing the volume fraction does not change the strain at which this occurs (point B) assuming constant IFSS.

When the IFSS is low (τ_c = 5 MPa), interfacial slippage (point A) occurs first followed by plasticity spread in the matrix (point B) as shown in Fig. 10. However, when using higher IFSS is used (i.e., when the interfacial bonding is improved), this order is switched, with plasticity occurring first followed by interfacial slippage. In this case, the effect of plasticity on the tangent stiffness reduction is more significant than the effect of interfacial shear slippage.

This result above means that improving the interface bonding strength leads to earlier development of "plasticity pockets" in the matrix due to the high concentration of shear stresses that result from stress-transfer between the matrix and the fiber. These "pockets" of plasticity lead to highly nonlinear behavior in the stress–strain behavior, as seen in Fig. 10 and as observed in test data on nano-composite. Such nonlinearity can augment the energy absorption capability while maintaining high stiffness of the composite.

5. Conclusions

A simplified approach for predicting the nonlinear stress–strain curve of unidirectional fibrous nano-composites is presented. The model, which incorporates interfacial shear stick–slip constitutive law and elasto-plastic matrix with isotropic strain hardening provides good results when compared against experimental data on aligned fibrous nano-composite. The study revealed that both stick–slip behavior and development of plasticity due to stress concentration contribute invariably to the nonlinear behavior of

the nano-composites. When the bond between the fiber and the matrix is very strong, plasticity spreads at lower strains, thus forming discrete "pockets of plasticity" in the composite. However, if the bond is weak, then slippage of the fibers within the composites causes nonlinear behavior of the composite. The combination of the two factors provide reasonable explanation for the improved and nonlinear behavior of nano-composite.

References

[1] Hu H, Onyebuekea L, Abatan A. Characterizing and modeling mechanical properties of nanocomposites – review and evaluation. J Miner Mater Charact Engi 2010;9(4):275–319.
[2] Holscher H, Schwarz UD, Zworner O, Wiesendanger R. Consequences of the stick–slip movement for the scanning force microscopy imaging of graphite. Phys Rev B 1998;57:2477–81.
[3] Buldum A, Lu JP. Atomic scale sliding and rolling of carbon nanotubes. Phys Rev Lett 1999;83:5050–3.
[4] Spitas V, Spitas C. Modelling of the elastic damping response of a carbon nanotube – polymer nanocomposite in the stress–strain domain using an elastic energy release approach based on stick–slip. Mech Adv Mater Struct, in press. pp. 1–17.
[5] Ajayan PM, Suhr J, Koratkar N. Utilizing interfaces in carbon nanotube reinforced polymer composites for structural damping. J Mater Sci 2006;41: 7824–9.
[6] Barber AH, Coshen S, Kenig S, Wagner HD. Interfacial fracture energy measurements for multi-walled carbon nanotubes pulled from a polymer matrix. Compos Sci Technol 2004;64:2283–9.
[7] Barber AH, Cohen SR, Eitan A, Schadler LS, Wagner HD. Fracture transitions at a carbon nanotube/polymer interface. Adv Mater 2006;18(1):83–7.
[8] Qian D, Dickey EC, Andrews R, Rantell T. Load transfer and deformation mechanisms in carbon nanotube-polystyrene composites. Appl Phys Lett 2000;76(20):2868–70.
[9] Hill R. Theory of mechanical properties of fibre-strengthened materials: I. Elastic behaviour. J Mech Phys Solids 1964;12:199–212.
[10] Halpin JC, Tsai SW. Effect of environmental factors on composite materials; air force technical report AFML-TR 67-423. Dayton (OH): Wright Aeronautical Laboratories; 1967.
[11] Halpin JC, Kardos JL. The Halpin-Tsai equations: a review. Polym Eng Sci 1976;16(5):344–51.
[12] Qu J, Cherkaoui M. Fundamental of micromechanics of solids. Hoboken, New Jersey: John Wiley & Sons, Inc.; 2006.
[13] Halpin JC. Stiffness and expansion estimates for oriented short fiber composites. J Compos Mater 1969;3:742–4.
[14] Tucker CL, Liang E. Stiffness predictions for unidirectional short-fiber composites: review and evaluation. Compos Sci Technol 1999;59(5): 655–71.
[15] Cox HL. The elasticity and strength of paper and other fibrous materials. Brit J Appl Phys 1952;3:72–9.
[16] Jahankhani H, Galiotis H. Interfacial shear stress distribution in model composites, Part 1: A Kevlar 49® fibre in an epoxy matrix. J Compos Mater 1991;25(5):609–31.
[17] Ogasawara T, Tsuda T, Takeda N. Stress–strain behavior of multi-walled carbon nanotube/PEEK composites. Compos Sci Technol 2011;71:73–8.
[18] Tasuda T, Ogasawara T, Deng F, Takeda N. Direct measurements of interfacial shear strength of multi-walled carbon nanotube/PEEK composite using a nano-pullout method. Comp Sci Technol 2011. http://dx.doi.org/10.1016/j.compscitech.2011.04.014.
[19] Erik T Thostenson, Chou Tsu-Wei. Aligned multi-walled carbon nanotube-reinforced composites: processing and mechanical characterization. J Phys D: Appl Phys 2002;35:L77–80.
[20] Sandler J, Werner P, Shaffer MSP, Demchuk V, Altstädt V, Windle AH. Carbon-nanofibre-reinforced poly(ether ether ketone) composites. Composites Part A 2002;33:1033–9.
[21] Zhang Yi, Suhir Ephraim, Yuan Xu. Effective Young's modulus of carbon nanofiber array. J Mater Res 2006;21(11):2948–54.